Human DDX6 regulates translation and decay of inefficiently translated mRNAs

Ramona Weber [1,2], Lara Wohlbold[1], and Chung-Te Chang [1,3,*]

[1] Department of Biochemistry, Max Planck Institute for Developmental Biology, Max-Planck-Ring 5, 72076 Tübingen, Germany

[2] Institute for Regenerative Medicine (IREM), University of Zurich, Wagistrasse 12, 8952 Schlieren-Zurich, Switzerland

[3] Institute of Biochemistry and Molecular Biology, National Yang Ming Chiao Tung University, Taipei City 112, Taiwan

* To whom correspondence should be addressed. Tel: +886 2 2826 7122; Fax: +886 2 2826 4843; Email: chungte.chang@nycu.edu.tw

ABSTRACT

Recent findings indicate that the translation elongation rate influences mRNA stability. One of the factors that has been implicated in this link between mRNA decay and translation speed is the yeast DEAD-box helicase Dhh1p. Here, we demonstrate that the human ortholog of Dhh1p, DDX6, triggers deadenylation-dependent decay of inefficiently translated mRNAs in human cells. DDX6 interacts with the ribosome through the Phe-Asp-Phe (FDF) motif in its RecA2 domain. Furthermore, RecA2-mediated interactions and ATPase activity are both required for DDX6 to destabilize inefficiently translated mRNAs. Using ribosome profiling and RNA sequencing, we identified two classes of endogenous mRNAs that are regulated in a DDX6-dependent manner. The identified targets are either translationally regulated or regulated at the steady-state-level and either exhibit signatures of poor overall translation or of locally reduced ribosome translocation rates. Transferring the identified sequence stretches into a reporter mRNA caused translation- and DDX6-dependent degradation of the reporter mRNA. In summary, these results identify DDX6 as a crucial regulator of mRNA translation and decay triggered by slow ribosome movement and provide insights into the mechanism by which DDX6 destabilizes inefficiently translated mRNAs.

INTRODUCTION

mRNA translation is a highly controlled process that critically determines the mRNA turnover rate. In particular, the elongation rate at which the ribosome translates an mRNA into the nascent peptide chain is thought to affect mRNA stability (D'Orazio and Green, 2021, Morris et al., 2021). Many mRNA attributes can affect the speed of the translating ribosome, including secondary structure (Doma and Parker, 2006), nucleotide and codon composition (Chaney and Clark, 2015, Gardin et al., 2014, Letzring et al., 2010), tRNA abundance (Ishimura et al., 2014, Novoa and Ribas de Pouplana, 2012, Nakahigashi et al., 2014), the sequence of the nascent peptide and its interaction with the ribosome exit tunnel or other ribosome-associated factors (Brandman et al., 2012, Charneski and Hurst, 2013, Kuroha et al., 2010, Tanner et al., 2009, Lin et al., 2020), and damage or improper processing of the mRNA itself (Brandman and Hegde, 2016, Joazeiro, 2019, Simms et al., 2017). It is now understood that recognition of slow ribosome dynamics by the mRNA decay machinery can trigger mRNA degradation, not only during ribosome-based quality control (RQC), but also in general translation regulation (Buskirk and Green, 2017, Buschauer et al., 2020, Radhakrishnan et al., 2016).

In eukaryotes, general mRNA decay is initiated by a shortening of the poly(A) tail mediated by the CCR4-NOT complex with its catalytic subunits CNOT7 and CNOT8, followed by 5′-to-3′ mRNA decay, where the mRNA is decapped by the DCP1/DCP2 decapping complex and then exonucleolytically degraded by the exonuclease XRN1 (Mugridge et al., 2018). Alternatively, the exosome can degrade deadenylated mRNA in the 3′-to-5′ direction (Robinson et al., 2015, Labno et al., 2016). There are also more specialized RQC mechanisms such as nonsense mediated decay, no-go decay, and non-stop decay which remove aberrant mRNAs often by endonucleolytic cleavage (Simms et al., 2017, Inada, 2017).

As mentioned above, mRNAs with slow translation rates due to the presence of non-optimal codons are regulated by translation-dependent decay (Radhakrishnan and Green, 2016, Richter and Coller, 2015, Presnyak et al., 2015, Boel et al., 2016, Herrick et al., 1990). One factor implicated in translation-dependent decay in yeast is Dhh1p, the ortholog of human DDX6 (Sweet et al., 2012, Radhakrishnan et al., 2016). DDX6 belongs to the conserved DEAD-box ATPase/helicase family, which plays a central role in cytoplasmic mRNA regulation, including processing body (P-body) assembly, mRNA decapping, and translational repression (Ostareck et al., 2014). DDX6 is composed of two globular RecA-like domains connected by a flexible linker. The helicase motifs that are crucial to the ATPase and RNA binding activities are located in the DDX6-RecA1 domain. The DDX6-RecA2 domain mediates binding to the translational regulators 4E-T and GIGYF1/2, the decapping activators PATL1, EDC3, LSM14A, and to the NOT1 subunit of the CCR4-NOT complex, thereby providing a link between mRNA translational repression and 5′-to-3′ mRNA decay by deadenylation and decapping (Mathys et al., 2014, Chen et al., 2014, Peter et al., 2019).

Despite its well-known involvement in translation-coupled RNA turnover in yeast, the target mRNAs and the molecular mechanism of mRNA recognition in mammalian DDX6 remain elusive. In this study, we investigated the role of human DDX6 in translation-dependent mRNA decay. Comparing the stability of a reporter mRNA containing a non-optimal codon stretch in both HEK293T WT and DDX6 KO cells revealed that DDX6 destabilizes inefficiently translated reporter mRNA in human cells, in a similar manner as has been observed in yeast (Radhakrishnan et al., 2016). The reporter is destabilized by initiation of 5′-to-3′ mRNA decay. Furthermore, we found that the DDX6 RecA2 domain interacts with ribosomal proteins and provide evidence that RecA2-mediated interactions and DDX6-ATPase activity are both necessary for translation-

dependent mRNA decay. To identify the set of inefficiently translated transcripts that are naturally targeted by DDX6 we took an unbiased approach and compared HEK293T-WT and -DDX6 KO cells by ribosome profiling and RNA sequencing analysis. This approach identified a set of mRNAs that are translationally regulated by DDX6, enriched in zinc finger transcription factors, and have low overall codon optimality and thus slow translation elongation dynamics across the entire open reading frame. We also identified a second group of mRNAs with locally decreased elongation dynamics targeted by DDX6 for decay. Interestingly, the second group of mRNAs included transcripts with CAG repeats, which have recently been linked to slow ribosome dynamics (Aviner et al., 2022). These findings suggest that loss of DDX6 could disrupt co-translational proteostasis of factors associated with neurodegenerative diseases, leading to the characteristic formation of intracellular aggregates. Through an mRNA reporter approach, we also found that the newly identified mRNA regions promote destabilization in a translation- and DDX6-dependent manner.

RESULTS

Codon composition affects mRNA stability in human cells

Codon optimality was recently identified as a strong determinant of mRNA stability in yeast, *Drosophila* and different vertebrate species (Presnyak et al., 2015, Bazzini et al., 2016, Mishima and Tomari, 2017). Since codon composition affects the ribosome translocation rate, it has been proposed that the translation elongation rate is monitored by the ribosome and ribosome-associated factors, triggering mRNA decay when the ribosome slows down (Hu et al., 2009, Sweet et al., 2012, Presnyak et al., 2015, Radhakrishnan and Green, 2016). To investigate this phenomenon in

more detail, we created a reporter construct containing a *Renilla* luciferase gene whose last thirty codons were replaced by synonymous but rarely used codons (Figure 1A). This change was designed to reduce the translation speed without altering the resulting protein sequence (Hussmann et al., 2015, Weinberg et al., 2016, Nakahigashi et al., 2014, Gardin et al., 2014, Yu et al., 2015, Letzring et al., 2010). To find out whether the expected decrease in ribosome translocation rates indeed alters mRNA stability, we measured the half-life of the reporter mRNA in human HEK293T cells. As expected, introducing the rare codon stretch into the *Renilla* luciferase open reading frame significantly reduced the half-life of its translated mRNA from > 10 h to 8.0 ± 4.4 h (Figure 1B,C). This result confirms that codon composition directly affects mRNA stability in human cells (Chen and Coller, 2016), and is in line with previous reports describing a correlation between codon optimality and RNA stability in various mammalian cell systems (Bazzini et al., 2016, Radhakrishnan and Green, 2016, Schwanhausser et al., 2011, Goodarzi et al., 2016).

In *Saccharomyces cerevisiae (S.c.)* the DEAD-box RNA helicase Dhh1p (ortholog of human DDX6) has been shown to act as a sensor of codon optimality (Sweet et al., 2012, Radhakrishnan et al., 2016). To test whether its human ortholog DDX6 is needed to trigger the decay of not optimally translated mRNAs, we created HEK293T DDX6 KO cells using CRISPR/Cas9-mediated gene editing. Loss of DDX6 protein expression was verified by western blotting and sequencing of the genomic target site (**Figure S1A,D; Experimental procedures**). Remarkably, loss of DDX6 significantly stabilized the non-optimal codon-containing reporter, resulting in a measured half-life comparable to that of the respective control reporter (> 10 h vs 8.0 ± 4.4 h) (**Figure 1B,C right panel**). These results indicate that DDX6 acts as a sensor of codon optimality and that this function is evolutionary conserved from yeast to mammals.

In budding and fission yeast, co-translational degradation of mRNA is mediated by the 5′-to-3′ decay pathway (Hu et al., 2009, Pelechano et al., 2015). It has also recently been reported that maternal codon-mediated mRNA clearance in zebrafish is triggered by co-translational CCR4-NOT-dependent deadenylation (Mishima and Tomari, 2017). To test whether the observed degradation of the rare-codon reporter is dependent on CCR4-NOT, we measured its half-life in cells overexpressing a catalytically inactive POP2 deadenylase mutant (POP2 DExAA). Blocking CCR4-NOT dependent deadenylation indeed resulted in marked stabilization of the reporter mRNA, with half-lives increasing from 5.5 ± 2.8 h to > 10 h (**Figure 1D,E**). This result shows that in human cells, mRNA decay triggered by rare codon-related slow ribosome movement is initiated by CCR4-NOT-dependent deadenylation of the target mRNA.

DDX6 interacts directly with the ribosome

To sense translation speed, it has been proposed that DDX6 must maintain physical interactions with the ribosome, and yeast Dhh1p has indeed been found to co-purify with ribosomal components (Radhakrishnan et al., 2016, Sweet et al., 2012, Drummond et al., 2011). To test whether human DDX6 interacts with the ribosome, we performed *in vitro* pulldown assays with recombinant DDX6 purified from *Escherichia coli* (*E.coli*) lysates, and endogenous ribosomal complex components purified from HEK293T cells. Streptavidin-tagged DDX6 pulled down several ribosomal protein components (labelled with a red dot), whereas no such interaction was observed in the corresponding streptavidin-MBP pulldown (**Figure 2A, lane 4 vs 6**). Interactions with ribosomal components therefore seem to be a conserved feature in DDX6 orthologs.

To determine precisely which part of DDX6 contacts the ribosome, we performed co-immunoprecipitations with DDX6 protein fragments in HEK293T cells. Since we did not know

which ribosomal component was mediating the interaction with DDX6, immunoprecipitations were performed in the presence of RNaseI. RNaseI cleaves unprotected internal RNA fragments but leaves the ribosome structure and ribosome-protected RNA regions intact (Ingolia et al., 2012). We found that under these conditions, overexpressed full length GFP-tagged DDX6 and the C-terminal RecA2 domain co-immunoprecipitated with both the HA-tagged large ribosomal subunit protein RPL22 and the small ribosomal subunit component RPS3A in human cells. In contrast, the N-terminal RecA1 domain did not interact with either subunits (**Figure 2B**). The RecA2 domain of DDX6 mediates multiple protein interactions. It binds the Mid domain of eIF4G (MIF4G) of NOT1 which stimulates its ATPase activity by stabilizing it in an activated conformation (Mathys et al., 2014, Chen et al., 2014). In addition to providing a link to the CCR4-NOT deadenylase complex, the RecA2 domain of DDX6 also mediates interactions with other regulatory proteins e.g. EDC3, LSM14A, PatL1, 4E-T and GIGYF1/2. These proteins interact with DDX6 RecA2 through their Phe-Asp-Phe (FDF) motifs in a mutually exclusive manner, thereby either facilitating mRNA decay by linking the deadenylation machinery to the core decapping complex or inducing translational repression (Fromm et al., 2012, Tritschler et al., 2008, Nissan et al., 2010, Sharif et al., 2013, Tritschler et al., 2009, Brandmann et al., 2018, Ozgur et al., 2015a, Peter et al., 2019).

To obtain further insights into how DDX6 interacts with the ribosome, we compared the interactions of different DDX6 mutants with the large ribosomal subunit protein RPL22 in HEK293T cells. In particular, we used a DDX6 mutant (Mut1; R94E + F101D + Q322A + N324A + R375A) that does not interact with NOT1 but still interacts with the FDF-binding pocket. We also tested a mutant with substitutions on the FDF-binding surface (Mut2; Q209A + H312A + T316A + R320A + R335A + K341A + K342A). These mutations prevent binding to regulatory factors such as EDC3, LSM14A, PatL1, 4E-T and GIGYF1/2, thereby breaking the link with the

decapping and translation repression machinery (Tritschler et al., 2009, Kuzuoglu-Ozturk et al., 2016, Ozgur et al., 2015a, Peter et al., 2019). As a control, we also tested a DDX6 DEAD-box mutant (E236Q). Interestingly, mutation of the FDF-binding surface abolished DDX6's interaction with the ribosomal protein RPL22, whereas mutations interrupting the interaction with NOT1 and mutation of the DEAD-box motif did not interfere with ribosome binding (**Figure 2C**). The DDX6 mutant with a modified FDF motif (Mut2) still interacted with NOT1, indicating that the fold was not compromised (**Figure 2C**). In summary, these results demonstrate that DDX6 interacts with the ribosome via the same region that provides a link to the decapping and translation repression machinery.

DDX6 belongs to the DEAD-box family of RNA dependent ATPases/helicases (Ozgur et al., 2015b, Presnyak and Coller, 2013, Russell et al., 2013). To test whether ATPase activity is required to promote the decay of rare-codon reporter mRNA, we complemented HEK293T DDX6 KO cells with either wild-type (WT) or DEAD-box mutant (E236Q) DDX6. Interestingly, loss of ATPase activity completely abolished DDX6's ability to induce decay of rare-codon reporter mRNA (**Figure 2D lane 2 vs lane 3 and 2E**). Sweet *et al.* found similarly that in yeast, Dhh1 interaction with polysomes following translation inhibition was dependent on its ATPase activity (Sweet et al., 2012).

To test whether the interactions mediated by the DDX6 RecA2 domain are also necessary for stalling mediated decay, we complemented DDX6 KO HEK293T cells with either the NOT1 binding mutant (Mut1) or FDF-pocket mutant (Mut2) of DDX6 and examined their effect on the stability of the non-optimal codon reporter. Stalling mediated mRNA decay was only observed in the presence of WT DDX6 (**Figure 2D lane 2 and 2E**). Loss of contact with NOT1 (Mut1) or of FDF-mediated interactions (Mut2) rendered DDX6 inactive (**Figure 2D lanes 4 and 5 and 2E**).

All proteins were expressed at equivalent levels (**Figure 2F**). These data show that DDX6 interacts with the ribosome via its C-terminal RecA2 domain and that all domains and its catalytic activity are required for it to mediate mRNA decay of a poorly translated reporter.

Identification of endogenous mRNAs targeted by DDX6 for decay because of inefficient translation elongation

To determine which cellular mRNAs are naturally sensed by DDX6 and targeted for decay, we performed ribosome profiling combined with RNA sequencing (RNA-seq) in HEK293T WT and DDX6 KO cells. Ribosome profiling involves high-throughput sequencing of the RNA footprints of polyribosomes subjected to *in vitro* RNA digestion (Ingolia et al., 2009, McGlincy and Ingolia, 2017). This technique can thus reveal genome-wide ribosomal occupancy with nucleotide resolution, providing insights into the number and position of ribosomes bound throughout the transcriptome (Ingolia et al., 2012). While the overall ribosomal occupancy on a given transcript gives a rough estimate of the amount of protein synthesized from that transcript, the distribution of ribosome occupancy within a transcript is a measure of local ribosome speed. In particular, ribosomal footprint counts tend to accumulate in sites where the ribosome passes more slowly than in the rest of the transcript, since the likelihood of catching that footprint in the steady-state snapshot of the ribosome profiling experiment increases (Ingolia et al., 2011). Ribosome profiling can therefore be used to study ribosomal pausing or stalling (Li et al., 2012, Guydosh and Green, 2014, Gamble et al., 2016). To investigate a possible link between locally increased ribosomal occupancy, indicative of slow ribosome elongation, and DDX6-dependent mRNA decay, we compared the RNA-seq and ribosome profiling data of HEK293T WT and HEK293T DDX6 KO cells (overview **Figure S2A**). Comparison of the two RNA-seq libraries revealed 1707 mRNAs

specifically upregulated in the absence of DDX6 (*FDR < 0.005;* **Figure 3A,C**). Of those, 298 transcripts were upregulated more than two-fold (logFC > 1). Gene ontology analysis revealed enrichment for transcripts coding for proteins that localize in the extracellular space, to membranes or are involved in signaling or in cell adhesion. On the other hand, 1484 transcripts were significantly downregulated (*FDR < 0.005;* **Figure 3A,C**), 156 more than two-fold (logFC < -1). In addition, comparing ribosome profiling and RNA-seq data allowed us to identify changes in translation efficiency (TE). Remarkably, 260 transcripts were translationally upregulated in DDX6 KO cells (*FDR < 0.005;* **Figure 3B,D**), 152 more than two-fold (logFC > 1). Functional characterization of these target genes revealed a predominance of genes encoding for zinc finger transcription factors (89 of the 260 translationally upregulated genes; 34%; FDR=2.5E-46) (**Figure 3B,D**). Accordingly, GO-analysis showed an enrichment for DNA binding proteins and factors involved in transcription (**Figure 3F**). In contrast, only 38 transcripts showed significant downregulation in TE (*FDR < 0.005;* **Figure 3B,D**), 17 more than two-fold (logFC < -1), with no functional association as measured by GO analysis. These results suggest that loss of DDX6 has a profound effect on the translation efficiency of a specific class of mRNAs and led us to investigate what molecular features the 260 mRNA targets translationally repressed by DDX6 have in common. Comparing the features of the 260 upregulated mRNAs in DDX6 KO cells revealed that these mRNAs have significantly lower coding sequence (CDS) GC content than the rest of the mRNAs expressed in the same cells (**Figure S3B**). Furthermore, DDX6 regulated CDSes appear to be longer than unaffected mRNA CDSs (**Figure S3C**). Interestingly, in mammals, low codon GC content is correlated with low codon optimality (Plotkin and Kudla, 2011). Thus, DDX6 may be involved in the regulation of the translation efficiency of mRNAs with low codon optimality across the whole transcriptome. DDX6 regulated mRNAs were not found to have a significantly

lower TE than the other mRNAs expressed in the cells; however, loss of DDX6 significantly increased the TE of this subset of mRNAs above the overall TE (**Figure S3D**).

In addition to the unexpected finding that DDX6 translationally represses a specific group of endogenous transcripts, we reasoned that we should also find potential targets of DDX6-mediated mRNA decay in the group of mRNAs that are more abundant in the absence of DDX6. Based on our previous observations that DDX6 mediates decay of inefficiently translated mRNAs, we further reasoned that we could use the ribosome profiling data to identify upregulated mRNAs with locally increased ribosome occupancy, indicative of slow elongation rates. We manually screened the list of transcripts with logFC > 1 and a statistically significant change (FDR < 0.005) in the RNA-seq experiment (298 transcripts) for the presence of locally increased ribosome footprint as measured by the coupled ribosome profiling experiment and found 35 genes that matched these criteria (**Table 1**). Note that one of the most highly upregulated mRNAs in DDX6 KO cells was the androgen receptor (AR) transcript containing GAC repeats, coding for a stretch of glutamine repeats (poly Q). The repetitive nature of this sequence makes it impossible to determine whether inefficient translation elongation occurs during synthesis. However, it is interesting to note that a recent preprint suggests CAG expansions can cause altered elongation kinetics that can lead to CAG expansion diseases like Huntington's disease (Aviner et al., 2022). Given the repetitive nature of the transcript, we hypothesize that AR could be a direct DDX6 target. We then used quantitative PCR (qPCR) to measure the levels of selected transcripts in WT, DDX6 KO cells and DDX6 KO cells expressing either WT or mutant DDX6 exogenously. DDX6 dependency was detected in 6 of the 9 tested mRNAs (**Figure 3G and S3A** AR, BMP2, LGALS1, DLX5, ENO2, PSMB9; see also changes in mRNA abundance as determined by RNA-seq; the remaining three potential DDX6 targets were not confirmed: C1QTNF4, CALCB, PCK1). We

observed that DDX6 KO cells had higher levels of targeted mRNAs compared to WT HEK293T cells, as revealed by RNA sequencing experiments, and were partially restored back to WT levels by overexpressing DDX6. The partial rescue might be explained by uneven transfection efficiency and/or additional time required to reach base line mRNA levels. It should be noted that none of the mutant forms of DDX6 were able to restore the endogenous levels of the targeted mRNA, consistent with the previous reporter experiments. All proteins were expressed at equivalent levels (**Figure 3H**). These results strongly suggest that DDX6 plays a direct role in the regulation of targeted mRNA levels in HEK293T cells.

mRNA sequences with increased ribosomal occupancy reduce reporter mRNA stability

To test whether the identified translational pause sites in some of the endogenous DDX6-targeted mRNAs contribute to mRNA destabilization, we created different reporter constructs in which the putative ribosomal stalling region (RSR) was inserted at the 3′ end of the Renilla luciferase open reading frame, either preceding or following a stop-codon; RL-RSR and RL-stop-RSR respectively (**Figure 4A**). These constructs were designed to differentiate translation dependent regulation from translation independent effects, triggered for example by binding of trans-regulatory factors (e.g. RNA-binding proteins or miRNAs) to the introduced sequence. We tested two of the sequences identified in our screen for DDX6-destabilized mRNAs: first, a stretch containing 23 'CAG' codon repeats (encoding 23 x Q) of the X-chromosome encoded AR gene. Repetitive codon sequences can lead to stalling because of limited tRNA availability (Dana and Tuller, 2014, Ishimura et al., 2014, Novoa and Ribas de Pouplana, 2012). For the second sequence, we chose a 30 nt-long fragment of the bone morphogenetic protein 2 (BMP2) gene encoded on chromosome 20, which codes for a sequence of basic amino acids (QRKRLKSSCK). Polybasic

amino acid stretches and prolines have been reported to cause ribosome stalling (Ingolia et al., 2011, Charneski and Hurst, 2013, Brandman et al., 2012). Since the sequence immediately adjacent to the actual stall site also contained several lysine, arginine and proline codons, we cloned the stalling sequence with ~100 nt upstream and downstream flanking to include all potential contributing regulatory element in the respective reporter constructs. We then measured the half-lives of the reporter constructs when transfected into HEK293T cells. For this, reporter mRNA was quantified by northern blot at different times after transcription was blocked using actinomycin D. As expected, presence of the *AR* stalling sequence before the stop-codon strongly reduced the mRNA half-life compared to the control vector where the stop-codon precedes the stalling sequence (**Figure 4B,C**). The same was true for the *BMP2* stalling sequence: presence of the stalling sequence was associated with a strong translation-dependent reduction in mRNA half-life (4.0 ± 1.9 h compared to > 10 h in the control vector) (**Figure 4D,E**). To prove that the observed reduction in reporter mRNA stability containing endogenous ribosomal stalling sites was dependent on DDX6, the half-life measurements were repeated in HEK293T DDX6 KO cells, and indeed, when expressed in DDX6 KO cells, the RL-stop and RL-vectors for both *AR* and *BMP2* stalling sequences had approximately similar half-lives (**Figure 4B-E**). These results therefore confirm that DDX6 is required to trigger the co-translational mRNA decay induced by these sequences.

To further confirm that the identified sequences of the *AR* and *BMP2* mRNAs lead to ribosome stalling, we performed RNA immunoprecipitation (RNA-IP) assays by pulling down the reporter RNA under DDX6 KO conditions and then detected the ribosome stalling level. In keeping with the mRNA half-life results, the reporters with the *AR* or *BMP2* stalling sequences pulled down increased amounts of HA-RPL22 in the RNA-IP assays (**Figure 4F**). In summary, using ribosome

profiling and follow up experiments, we were able to identify endogenous sequences with reduced elongation rates that trigger co-translational mRNA decay in a DDX6-dependent manner in human cells.

Discussion

mRNA decay factors regulate gene expression by processes other than just general mRNA degradation. For example, it has recently been shown that the translational elongation rate influences mRNA stability. One factor implicated in coupling mRNA decay with translation rates is the yeast decay factor, Dhh1p. In this study, we show that mRNA stability in human cells is also affected by codon optimality, just as it is in yeast. Moreover, DDX6 (the human ortholog of Dhh1p) plays an important role in triggering the decay of slowly translated mRNAs. Using a wide range of approaches, we systematically characterized the contribution of DDX6 to ribosome stalling-mediated mRNA decay.

To investigate whether DDX6 is necessary to trigger the decay of sub-optimally translated mRNA, we created a reporter construct containing a *Renilla* luciferase open reading frame where the last thirty codons were replaced by synonymous but rarely used codons, chosen to reduce the translation rate without altering the protein sequence produced. The reporter with the non-optimal codons was much more stable in the absence of DDX6, with a half-life comparable to that of the corresponding WT reporter. This result demonstrates that DDX6 acts as sensor of codon optimality and that this function is evolutionarily conserved from yeast to mammals. We also demonstrated that DDX6 interacts directly with the ribosome through the RecA2 domain, which also binds to the CCR4-NOT complex. By overexpressing DDX6 mutants in DDX6 KO cells, we showed that DDX6-CCR4-NOT interactions are essential for ribosome stalling-dependent mRNA decay.

To identify a possible link between increased ribosomal occupancy and DDX6-dependent mRNA decay, we performed RNA-seq and ribosome profiling experiments in HEK293T WT and DDX6 KO cells. Comparison of the two RNA-seq libraries allowed us to identify mRNAs that are upregulated in the absence of DDX6. These DDX6-regulated mRNA targets were further examined using ribosome profiling and found to have increased ribosome occupancy in specific regions, indicative of slow ribosome movement, which may therefore destabilize the corresponding mRNAs. Importantly, we also found that reporter mRNAs containing the ribosomal stalling region were only destabilized in the presence of both translation and DDX6.

These findings have important implications for understanding the regulation of gene expression and the underlying mechanisms of mRNA decay. By elucidating the role of DDX6 and the CCR4-NOT complex in this process, we may be able to develop more effective therapeutic strategies for diseases caused by dysregulated gene expression. Furthermore, the approach used here of combining RNA-seq and ribosome profiling technologies could be applied to other biological systems to gain a deeper understanding of the molecular mechanisms underlying translation-coupled mRNA decay. Overall, our work opens up exciting avenues for future research and could potentially contribute to the development of novel treatments for a variety of diseases.

ACKNOWLEDGMENTS

We dedicate this work to the memory of Elisa Izaurralde who passed away while this work was still ongoing. We thank Catrin Weiler, Sigrun Helms and Heike Budde for excellent technical assistance. We are very grateful to Estienne Swart for insightful comments on the manuscript.

This work was supported by the Higher Education Sprout Project of the National Yang Ming Chiao Tung University and Ministry of Education (MOE), Taiwan.

FUNDING

This work was supported by the Max Planck Society, the National Science and Technology Council, Taiwan [NSTC111-2311-B-A49-005-], and the Yen Tjing Ling Medical Foundation [CI-112-13].

AUTHOR CONTRIBUTION

Conceptualization, C.C. and E.I.; Methodology, C.C., R.W., L.W.; Investigation, C.C., R.W., L.W.; Project administration, C.C., R.W. and L.W.; Writing, L.W., C.C. and R.W.

CONFLICT OF INTEREST

None declared.

MATERIAL AND METHODS

Generation of a HEK293T DDX6 KO cell line

The knock-out of DDX6 in HEK293T cells was generated by CRISPR-Cas9. The guide RNA targeting Exon 3 of DDX6 (5′- GTCTTTTTCCAGTCATCACC -3′) was designed using DNA2.0 (ATUM) online tool to minimize off-target effects. Targeting resulted in a 1 nucleotide insertion in one allele and a 10 nucleotides deletion in the other allele, both causing a frameshift of the open reading frame.

Northern blotting and quantification

For detection of the RNA half-life, HEK293T wild-type or DDX6 KO cells in 6-well plate were transfected with the 0.5 µg indicated *Renilla* luciferase (RL) reporter plasmid. 48 hours after transfection, the RL reporter mRNA level was monitored following inhibition of transcription by actinomycin D and then isolated using Trizol Reagent (Thermo) and analyzed by Northern blot as described previously (Braun et al., 2011). RL reporter mRNA levels were then normalized to 18S rRNA and plotted against time and calculated the mRNA half-lives ($t_{1/2}$) ± standard deviations from the decay curves.

Ribosomal proteins purification from HEK293T cells

The method to purify ribosomal proteins from HEK293T cells was adapted from previously published protocol (Belin et al., 2010). In brief, HEK293T cells are submitted to an osmotic shock by incubation in an appropriate hypotonic buffer containing NP-40. After removing the nuclear fraction by centrifugation at 750 g, the cytoplasmic fraction is further submitted to centrifugation at 12,500 g to remove the mitochondrial fraction. The concentration of the post-mitochondrial fraction is then adjusted to 0.5 M KCl to disrupt most interactions between ribosomes and other proteins of the other cell compartments. Finally, ribosomes are purified

through a sucrose cushion by ultracentrifugation. Purified ribosomes are ready for the subsequent analyses.

Pulldown assay

NusA-Strep-tagged DDX6 was produced in *E. coli* BL21(DE3) Star cells (Thermo Fisher) in LB medium at 20 °C. For the purification, cells were lysed by sonication in PBST buffer. NusA-Strep-tagged DDX6 was isolated from the crude lysate on Strep-Tactin sepharose (IBA) resin for 1 hr at 4 °C. The resin was then washed twice with lysis buffer and once with binding buffer [50 mM Tris/HCl (pH 7.5), 150 mM NaCl]. Purified human ribosome proteins were then added to the resin and incubated for 1 hr at 4 °C. After three washes with the binding buffer, bound proteins were eluted with 2x protein sample buffer and analyzed by SDS-PAGE following Coomassie staining.

Immunoprecipitation assay

HEK293T cells were grown in 10-cm dishes and transfected using Lipofectamine 2000 (Invitrogen). The transfection mixtures contained 10 μg of GFP- and HA-tagged constructs. HEK293T cells were harvested 48 hours after transfection. CoIPs and western blots were performed as described previously (Chang et al., 2014). HA- and GFP-tagged proteins were detected using horseradish peroxidase–conjugated monoclonal anti-HA (Roche, 3F10, 1:5,000) and anti-GFP (Roche, 11814460001, 1:2,000), respectively. Endogenous human RPS3A was detected using a polyclonal anti-RPS3A antibody (abcam, ab264368, 1:1,000), and CNOT1 was detected using a rabbit anti-CNOT1 antibody (in house, 1:1,000).

Reporter based ribosomal proteins enrichment assay

HEK293T cells were plated in a 10 cm dish at 80% confluence. Indicated RL reporter, HA-tagged RPL22 and MS2-HA-strep plasmids were transfected into HEK293T cells. After 48 hr, the cells were collected and washed once with pre-cooled PBS. Cells were then lysed in NET

buffer (50 mM Tris, pH 7.4, 1 mM EDTA, 150 mM NaCl, 0.1% Triton X-100). The lysate was centrifuged for 5 min at 13000 g, 4°C. The Supernatant was incubated with Strep-Tactin sepharose (IBA) resin with/without RNase A for 1 hr at 4°C. After three washes with NET buffer, bound proteins were eluted with 2x protein sample buffer and analyzed by western blots.

RNA-seq and ribosome profiling

For RNA and **ribosome profiling experiments** HEK293T wild-type or DDX6 KO were plated on 15cm dishes 24 hours before harvesting. Cells were harvested as described in (Calviello et al., 2016). For total RNA libraries, RNA was extracted using the RNeasy Mini Kit (Qiagen) and processed according to the Illumina TruSeq RNA Sample Prep Kit. For **ribosome profiling** the original protocol (Ingolia et al., 2012) was used in a modified version described in (Calviello et al., 2016).

RNA-seq and ribosome profiling libraries were sequenced on an Illumina Hiseq3000 instrument. Reads originating from ribosomal RNA were removed using Bowtie2 (Langmead and Salzberg, 2012). Remaining reads were mapped onto the human genome using Tophat2 (Kim et al., 2013) which resulted in 21-27 million mapped reads with an overall read mapping rate >91% for RNA-Seq and 3-4 million mapped reads with an overall read mapping rate >87% for Ribo-Seq. Read count analysis was performed using QuasR (Gaidatzis et al., 2015), differential expression analysis was performed using edgeR (Robinson et al., 2010, McCarthy et al., 2012). Translational efficiencies (TE) were calculated using RiboDiff (Zhong et al., 2017).

DDX6 stalling-induced decay targets were selected I. based on the logFC of total RNA of DDX6 KO versus WT HEK293T cells. Targets with a logFC>1 and statistical significant change FDR<0.005 (n=298) were manually screened for potential stalling sites using the Integrative Genomics Viewer tool from Broad Institute (Robinson et al., 2011, Thorvaldsdottir et al., 2013)

II. Stalling targets were selected based on a local accumulation of footprints determined by ribosome profiling. We found 35 genes that matched these criteria (AMDHD2, AR, ART5, BMP2, C1QTNF4, CA11, CALCB, CD19, CILP2, COL2A1, CTSA, CXCL12, DLX5, DUSP1, ENO2, HOXA13, IFI35, IFITM2, IGFBP5, LGALS1, MLC1, PBXIP1, PCK1, PSMB9, PTRH1, QPCT, SAT1, SEMA6C, SFXN3, SLC13A4, SLIT2, SMPDL3B, TMSB15B, TNC, ZNF91). A representation of the most convincing targets (AR, BMP2, LGALS1, DLX5, ENO2, PSMB9) can be found in Figure S2B-G.

GO analysis was performed using the R-based package goseq (Young et al., 2010). Analyses of GC content, CDS length and transcript TE were performed with R-based scripts.

Reverse transcription (RT) and quantitative PCR (qPCR)

We used quantitative PCR (qPCR) to determine transcript levels of selected targets. 22nt primers were designed using Primer-BLAST from NCBI to amplify a 250-350bp region of the target mRNA. To use the Livak method (ΔΔCT method) for relative quantification each primer pair was tested if the amplification rate of the specific PCR product is 2 +/- 5%.

For validation and rescue experiments HEK293T wild-type or DDX6 KO cells were either transfected with a GFP-MBP control or GFP-DDX6 (either WT, Mut1, Mut2, DEAD*). 48h after transfection total RNA was extracted and reverse transcribed using random hexamer primers. Target mRNA amount was subsequently determined by qPCR using the respective primer pair and normalized to beta-Actin abundance in the same sample. A sample treated with water instead of reverse transcriptase (-RT) was used as a negative control. Relative abundances of target mRNAs of three independent experiment were determined using the Livak method (the wild-type sample was arbitrarily set to 1) (Livak and Schmittgen, 2001).

Data availability

The datasets generated in this study have been deposited in the NCBI Gene Expression Omnibus (GEO) with the accession number GSE231964.

REFERENCES

AVINER, R., LEE, T.-T., MASTO, V. B., GESTAUT, D., LI, K. H., ANDINO, R. & FRYDMAN, J. 2022. Ribotoxic collisions on CAG expansions disrupt proteostasis and stress responses in Huntington's Disease. *bioRxiv*.

BAZZINI, A. A., DEL VISO, F., MORENO-MATEOS, M. A., JOHNSTONE, T. G., VEJNAR, C. E., QIN, Y., YAO, J., KHOKHA, M. K. & GIRALDEZ, A. J. 2016. Codon identity regulates mRNA stability and translation efficiency during the maternal-to-zygotic transition. *EMBO J,* 35**,** 2087-2103.

BELIN, S., HACOT, S., DAUDIGNON, L., THERIZOLS, G., POURPE, S., MERTANI, H. C., ROSA-CALATRAVA, M. & DIAZ, J. J. 2010. Purification of ribosomes from human cell lines. *Curr Protoc Cell Biol,* Chapter 3**,** Unit 3 40.

BOEL, G., LETSO, R., NEELY, H., PRICE, W. N., WONG, K. H., SU, M., LUFF, J., VALECHA, M., EVERETT, J. K., ACTON, T. B., XIAO, R., MONTELIONE, G. T., AALBERTS, D. P. & HUNT, J. F. 2016. Codon influence on protein expression in E. coli correlates with mRNA levels. *Nature,* 529**,** 358-363.

BRANDMAN, O. & HEGDE, R. S. 2016. Ribosome-associated protein quality control. *Nat Struct Mol Biol,* 23**,** 7-15.

BRANDMAN, O., STEWART-ORNSTEIN, J., WONG, D., LARSON, A., WILLIAMS, C. C., LI, G. W., ZHOU, S., KING, D., SHEN, P. S., WEIBEZAHN, J., DUNN, J. G., ROUSKIN, S., INADA, T., FROST, A. & WEISSMAN, J. S. 2012. A ribosome-bound quality control complex triggers degradation of nascent peptides and signals translation stress. *Cell,* 151**,** 1042-54.

BRANDMANN, T., FAKIM, H., PADAMSI, Z., YOUN, J. Y., GINGRAS, A. C., FABIAN, M. R. & JINEK, M. 2018. Molecular architecture of LSM14 interactions involved in the assembly of mRNA silencing complexes. *EMBO J,* 37.

BRAUN, J. E., HUNTZINGER, E., FAUSER, M. & IZAURRALDE, E. 2011. GW182 proteins directly recruit cytoplasmic deadenylase complexes to miRNA targets. *Mol Cell,* 44**,** 120-33.

BUSCHAUER, R., MATSUO, Y., SUGIYAMA, T., CHEN, Y. H., ALHUSAINI, N., SWEET, T., IKEUCHI, K., CHENG, J., MATSUKI, Y., NOBUTA, R., GILMOZZI, A., BERNINGHAUSEN, O., TESINA, P., BECKER, T., COLLER, J., INADA, T. & BECKMANN, R. 2020. The Ccr4-Not complex monitors the translating ribosome for codon optimality. *Science,* 368.

BUSKIRK, A. R. & GREEN, R. 2017. Ribosome pausing, arrest and rescue in bacteria and eukaryotes. *Philos Trans R Soc Lond B Biol Sci,* 372.

CALVIELLO, L., MUKHERJEE, N., WYLER, E., ZAUBER, H., HIRSEKORN, A., SELBACH, M., LANDTHALER, M., OBERMAYER, B. & OHLER, U. 2016. Detecting actively translated open reading frames in ribosome profiling data. *Nat Methods,* 13**,** 165-70.

CHANEY, J. L. & CLARK, P. L. 2015. Roles for Synonymous Codon Usage in Protein Biogenesis. *Annu Rev Biophys,* 44**,** 143-66.

CHANG, C. T., BERCOVICH, N., LOH, B., JONAS, S. & IZAURRALDE, E. 2014. The activation of the decapping enzyme DCP2 by DCP1 occurs on the EDC4 scaffold and involves a conserved loop in DCP1. *Nucleic Acids Res,* 42**,** 5217-33.

CHARNESKI, C. A. & HURST, L. D. 2013. Positively charged residues are the major determinants of ribosomal velocity. *PLoS Biol,* 11**,** e1001508.

CHEN, Y., BOLAND, A., KUZUOGLU-OZTURK, D., BAWANKAR, P., LOH, B., CHANG, C. T., WEICHENRIEDER, O. & IZAURRALDE, E. 2014. A DDX6-CNOT1 complex and W-binding pockets in CNOT9 reveal direct links between miRNA target recognition and silencing. *Mol Cell,* 54**,** 737-50.

CHEN, Y. H. & COLLER, J. 2016. A Universal Code for mRNA Stability? *Trends Genet,* 32**,** 687-688.

D'ORAZIO, K. N. & GREEN, R. 2021. Ribosome states signal RNA quality control. *Mol Cell,* 81**,** 1372-1383.

DANA, A. & TULLER, T. 2014. The effect of tRNA levels on decoding times of mRNA codons. *Nucleic Acids Res,* 42**,** 9171-81.

DOMA, M. K. & PARKER, R. 2006. Endonucleolytic cleavage of eukaryotic mRNAs with stalls in translation elongation. *Nature,* 440**,** 561-4.

DRUMMOND, S. P., HILDYARD, J., FIRCZUK, H., REAMTONG, O., LI, N., KANNAMBATH, S., CLAYDON, A. J., BEYNON, R. J., EYERS, C. E. & MCCARTHY, J. E. 2011. Diauxic shift-dependent relocalization of decapping activators Dhh1 and Pat1 to polysomal complexes. *Nucleic Acids Res,* 39**,** 7764-74.

FROMM, S. A., TRUFFAULT, V., KAMENZ, J., BRAUN, J. E., HOFFMANN, N. A., IZAURRALDE, E. & SPRANGERS, R. 2012. The structural basis of Edc3- and Scd6-mediated activation of the Dcp1:Dcp2 mRNA decapping complex. *EMBO J,* 31**,** 279-90.

GAIDATZIS, D., LERCH, A., HAHNE, F. & STADLER, M. B. 2015. QuasR: quantification and annotation of short reads in R. *Bioinformatics,* 31**,** 1130-2.

GAMBLE, C. E., BRULE, C. E., DEAN, K. M., FIELDS, S. & GRAYHACK, E. J. 2016. Adjacent Codons Act in Concert to Modulate Translation Efficiency in Yeast. *Cell,* 166**,** 679-690.

GARDIN, J., YEASMIN, R., YUROVSKY, A., CAI, Y., SKIENA, S. & FUTCHER, B. 2014. Measurement of average decoding rates of the 61 sense codons in vivo. *Elife,* 3.

GOODARZI, H., NGUYEN, H. C. B., ZHANG, S., DILL, B. D., MOLINA, H. & TAVAZOIE, S. F. 2016. Modulated Expression of Specific tRNAs Drives Gene Expression and Cancer Progression. *Cell,* 165**,** 1416-1427.

GUYDOSH, N. R. & GREEN, R. 2014. Dom34 rescues ribosomes in 3' untranslated regions. *Cell,* 156**,** 950-62.

HERRICK, D., PARKER, R. & JACOBSON, A. 1990. Identification and comparison of stable and unstable mRNAs in Saccharomyces cerevisiae. *Mol Cell Biol,* 10**,** 2269-84.

HU, W., SWEET, T. J., CHAMNONGPOL, S., BAKER, K. E. & COLLER, J. 2009. Co-translational mRNA decay in Saccharomyces cerevisiae. *Nature,* 461**,** 225-9.

HUSSMANN, J. A., PATCHETT, S., JOHNSON, A., SAWYER, S. & PRESS, W. H. 2015. Understanding Biases in Ribosome Profiling Experiments Reveals Signatures of Translation Dynamics in Yeast. *PLoS Genet,* 11**,** e1005732.

INADA, T. 2017. The Ribosome as a Platform for mRNA and Nascent Polypeptide Quality Control. *Trends Biochem Sci,* 42**,** 5-15.

INGOLIA, N. T., BRAR, G. A., ROUSKIN, S., MCGEACHY, A. M. & WEISSMAN, J. S. 2012. The ribosome profiling strategy for monitoring translation in vivo by deep sequencing of ribosome-protected mRNA fragments. *Nat Protoc,* 7**,** 1534-50.

INGOLIA, N. T., GHAEMMAGHAMI, S., NEWMAN, J. R. & WEISSMAN, J. S. 2009. Genome-wide analysis in vivo of translation with nucleotide resolution using ribosome profiling. *Science,* 324**,** 218-23.

INGOLIA, N. T., LAREAU, L. F. & WEISSMAN, J. S. 2011. Ribosome profiling of mouse embryonic stem cells reveals the complexity and dynamics of mammalian proteomes. *Cell,* 147**,** 789-802.

ISHIMURA, R., NAGY, G., DOTU, I., ZHOU, H., YANG, X. L., SCHIMMEL, P., SENJU, S., NISHIMURA, Y., CHUANG, J. H. & ACKERMAN, S. L. 2014. RNA function. Ribosome stalling induced by mutation of a CNS-specific tRNA causes neurodegeneration. *Science,* 345**,** 455-9.

JOAZEIRO, C. A. P. 2019. Mechanisms and functions of ribosome-associated protein quality control. *Nat Rev Mol Cell Biol,* 20**,** 368-383.

KIM, D., PERTEA, G., TRAPNELL, C., PIMENTEL, H., KELLEY, R. & SALZBERG, S. L. 2013. TopHat2: accurate alignment of transcriptomes in the presence of insertions, deletions and gene fusions. *Genome Biol,* 14**,** R36.

KUROHA, K., AKAMATSU, M., DIMITROVA, L., ITO, T., KATO, Y., SHIRAHIGE, K. & INADA, T. 2010. Receptor for activated C kinase 1 stimulates nascent polypeptide-dependent translation arrest. *EMBO Rep,* 11**,** 956-61.

KUZUOGLU-OZTURK, D., BHANDARI, D., HUNTZINGER, E., FAUSER, M., HELMS, S. & IZAURRALDE, E. 2016. miRISC and the CCR4-NOT complex silence mRNA targets independently of 43S ribosomal scanning. *EMBO J,* 35**,** 1186-203.

LABNO, A., TOMECKI, R. & DZIEMBOWSKI, A. 2016. Cytoplasmic RNA decay pathways - Enzymes and mechanisms. *Biochim Biophys Acta,* 1863**,** 3125-3147.

LANGMEAD, B. & SALZBERG, S. L. 2012. Fast gapped-read alignment with Bowtie 2. *Nat Methods,* 9**,** 357-9.
LETZRING, D. P., DEAN, K. M. & GRAYHACK, E. J. 2010. Control of translation efficiency in yeast by codon-anticodon interactions. *RNA,* 16**,** 2516-28.
LI, G. W., OH, E. & WEISSMAN, J. S. 2012. The anti-Shine-Dalgarno sequence drives translational pausing and codon choice in bacteria. *Nature,* 484**,** 538-41.
LIN, Z., GASIC, I., CHANDRASEKARAN, V., PETERS, N., SHAO, S., MITCHISON, T. J. & HEGDE, R. S. 2020. TTC5 mediates autoregulation of tubulin via mRNA degradation. *Science,* 367**,** 100-104.
LIVAK, K. J. & SCHMITTGEN, T. D. 2001. Analysis of relative gene expression data using real-time quantitative PCR and the 2(-Delta Delta C(T)) Method. *Methods,* 25**,** 402-8.
MATHYS, H., BASQUIN, J., OZGUR, S., CZARNOCKI-CIECIURA, M., BONNEAU, F., AARTSE, A., DZIEMBOWSKI, A., NOWOTNY, M., CONTI, E. & FILIPOWICZ, W. 2014. Structural and biochemical insights to the role of the CCR4-NOT complex and DDX6 ATPase in microRNA repression. *Mol Cell,* 54**,** 751-65.
MCCARTHY, D. J., CHEN, Y. & SMYTH, G. K. 2012. Differential expression analysis of multifactor RNA-Seq experiments with respect to biological variation. *Nucleic Acids Res,* 40**,** 4288-97.
MCGLINCY, N. J. & INGOLIA, N. T. 2017. Transcriptome-wide measurement of translation by ribosome profiling. *Methods,* 126**,** 112-129.
MISHIMA, Y. & TOMARI, Y. 2017. Pervasive yet nonuniform contributions of Dcp2 and Cnot7 to maternal mRNA clearance in zebrafish. *Genes Cells,* 22**,** 670-678.
MORRIS, C., CLUET, D. & RICCI, E. P. 2021. Ribosome dynamics and mRNA turnover, a complex relationship under constant cellular scrutiny. *Wiley Interdiscip Rev RNA***,** e1658.
MUGRIDGE, J. S., COLLER, J. & GROSS, J. D. 2018. Structural and molecular mechanisms for the control of eukaryotic 5'-3' mRNA decay. *Nat Struct Mol Biol,* 25**,** 1077-1085.
NAKAHIGASHI, K., TAKAI, Y., SHIWA, Y., WADA, M., HONMA, M., YOSHIKAWA, H., TOMITA, M., KANAI, A. & MORI, H. 2014. Effect of codon adaptation on codon-level and gene-level translation efficiency in vivo. *BMC Genomics,* 15**,** 1115.
NISSAN, T., RAJYAGURU, P., SHE, M., SONG, H. & PARKER, R. 2010. Decapping activators in Saccharomyces cerevisiae act by multiple mechanisms. *Mol Cell,* 39**,** 773-83.
NOVOA, E. M. & RIBAS DE POUPLANA, L. 2012. Speeding with control: codon usage, tRNAs, and ribosomes. *Trends Genet,* 28**,** 574-81.
OSTARECK, D. H., NAARMANN-DE VRIES, I. S. & OSTARECK-LEDERER, A. 2014. DDX6 and its orthologs as modulators of cellular and viral RNA expression. *Wiley Interdiscip Rev RNA,* 5**,** 659-78.
OZGUR, S., BASQUIN, J., KAMENSKA, A., FILIPOWICZ, W., STANDART, N. & CONTI, E. 2015a. Structure of a Human 4E-T/DDX6/CNOT1 Complex Reveals the Different Interplay of DDX6-Binding Proteins with the CCR4-NOT Complex. *Cell Rep,* 13**,** 703-711.
OZGUR, S., BUCHWALD, G., FALK, S., CHAKRABARTI, S., PRABU, J. R. & CONTI, E. 2015b. The conformational plasticity of eukaryotic RNA-dependent ATPases. *FEBS J,* 282**,** 850-63.
PELECHANO, V., WEI, W. & STEINMETZ, L. M. 2015. Widespread Co-translational RNA Decay Reveals Ribosome Dynamics. *Cell,* 161**,** 1400-12.
PETER, D., RUSCICA, V., BAWANKAR, P., WEBER, R., HELMS, S., VALKOV, E., IGREJA, C. & IZAURRALDE, E. 2019. Molecular basis for GIGYF-Me31B complex assembly in 4EHP-mediated translational repression. *Genes Dev,* 33**,** 1355-1360.
PLOTKIN, J. B. & KUDLA, G. 2011. Synonymous but not the same: the causes and consequences of codon bias. *Nat Rev Genet,* 12**,** 32-42.
PRESNYAK, V., ALHUSAINI, N., CHEN, Y. H., MARTIN, S., MORRIS, N., KLINE, N., OLSON, S., WEINBERG, D., BAKER, K. E., GRAVELEY, B. R. & COLLER, J. 2015. Codon optimality is a major determinant of mRNA stability. *Cell,* 160**,** 1111-24.
PRESNYAK, V. & COLLER, J. 2013. The DHH1/RCKp54 family of helicases: an ancient family of proteins that promote translational silencing. *Biochim Biophys Acta,* 1829**,** 817-23.

RADHAKRISHNAN, A., CHEN, Y. H., MARTIN, S., ALHUSAINI, N., GREEN, R. & COLLER, J. 2016. The DEAD-Box Protein Dhh1p Couples mRNA Decay and Translation by Monitoring Codon Optimality. *Cell,* 167**,** 122-132 e9.

RADHAKRISHNAN, A. & GREEN, R. 2016. Connections Underlying Translation and mRNA Stability. *J Mol Biol,* 428**,** 3558-64.

RICHTER, J. D. & COLLER, J. 2015. Pausing on Polyribosomes: Make Way for Elongation in Translational Control. *Cell,* 163**,** 292-300.

ROBINSON, J. T., THORVALDSDOTTIR, H., WINCKLER, W., GUTTMAN, M., LANDER, E. S., GETZ, G. & MESIROV, J. P. 2011. Integrative genomics viewer. *Nat Biotechnol,* 29**,** 24-6.

ROBINSON, M. D., MCCARTHY, D. J. & SMYTH, G. K. 2010. edgeR: a Bioconductor package for differential expression analysis of digital gene expression data. *Bioinformatics,* 26**,** 139-40.

ROBINSON, S. R., OLIVER, A. W., CHEVASSUT, T. J. & NEWBURY, S. F. 2015. The 3' to 5' Exoribonuclease DIS3: From Structure and Mechanisms to Biological Functions and Role in Human Disease. *Biomolecules,* 5**,** 1515-39.

RUSSELL, R., JARMOSKAITE, I. & LAMBOWITZ, A. M. 2013. Toward a molecular understanding of RNA remodeling by DEAD-box proteins. *RNA Biol,* 10**,** 44-55.

SCHWANHAUSSER, B., BUSSE, D., LI, N., DITTMAR, G., SCHUCHHARDT, J., WOLF, J., CHEN, W. & SELBACH, M. 2011. Global quantification of mammalian gene expression control. *Nature,* 473**,** 337-42.

SHARIF, H., OZGUR, S., SHARMA, K., BASQUIN, C., URLAUB, H. & CONTI, E. 2013. Structural analysis of the yeast Dhh1-Pat1 complex reveals how Dhh1 engages Pat1, Edc3 and RNA in mutually exclusive interactions. *Nucleic Acids Res,* 41**,** 8377-90.

SIMMS, C. L., THOMAS, E. N. & ZAHER, H. S. 2017. Ribosome-based quality control of mRNA and nascent peptides. *Wiley Interdiscip Rev RNA,* 8.

SWEET, T., KOVALAK, C. & COLLER, J. 2012. The DEAD-box protein Dhh1 promotes decapping by slowing ribosome movement. *PLoS Biol,* 10**,** e1001342.

TANNER, D. R., CARIELLO, D. A., WOOLSTENHULME, C. J., BROADBENT, M. A. & BUSKIRK, A. R. 2009. Genetic identification of nascent peptides that induce ribosome stalling. *J Biol Chem,* 284**,** 34809-18.

THORVALDSDOTTIR, H., ROBINSON, J. T. & MESIROV, J. P. 2013. Integrative Genomics Viewer (IGV): high-performance genomics data visualization and exploration. *Brief Bioinform,* 14**,** 178-92.

TRITSCHLER, F., BRAUN, J. E., EULALIO, A., TRUFFAULT, V., IZAURRALDE, E. & WEICHENRIEDER, O. 2009. Structural basis for the mutually exclusive anchoring of P body components EDC3 and Tral to the DEAD box protein DDX6/Me31B. *Mol Cell,* 33**,** 661-8.

TRITSCHLER, F., EULALIO, A., HELMS, S., SCHMIDT, S., COLES, M., WEICHENRIEDER, O., IZAURRALDE, E. & TRUFFAULT, V. 2008. Similar modes of interaction enable Trailer Hitch and EDC3 to associate with DCP1 and Me31B in distinct protein complexes. *Mol Cell Biol,* 28**,** 6695-708.

WEINBERG, D. E., SHAH, P., EICHHORN, S. W., HUSSMANN, J. A., PLOTKIN, J. B. & BARTEL, D. P. 2016. Improved Ribosome-Footprint and mRNA Measurements Provide Insights into Dynamics and Regulation of Yeast Translation. *Cell Rep,* 14**,** 1787-1799.

YOUNG, M. D., WAKEFIELD, M. J., SMYTH, G. K. & OSHLACK, A. 2010. Gene ontology analysis for RNA-seq: accounting for selection bias. *Genome Biol,* 11**,** R14.

YU, C. H., DANG, Y., ZHOU, Z., WU, C., ZHAO, F., SACHS, M. S. & LIU, Y. 2015. Codon Usage Influences the Local Rate of Translation Elongation to Regulate Co-translational Protein Folding. *Mol Cell,* 59**,** 744-54.

ZHONG, Y., KARALETSOS, T., DREWE, P., SREEDHARAN, V. T., KUO, D., SINGH, K., WENDEL, H. G. & RATSCH, G. 2017. RiboDiff: detecting changes of mRNA translation efficiency from ribosome footprints. *Bioinformatics,* 33**,** 139-141.

FIGURE LEGENDS

Figure 1 DDX6 functions as a sensor of rare codon-triggered mRNA decay in human cells

A. Schematic representation of the reporters used in panels (B, D).

B. Wild-type (WT) and DDX6 KO HEK293T cells were transfected with indicated reporter plasmids. After 48 hr, cells were treated with actinomycin D (ActD) and harvested at the indicated time points. Reporter mRNA levels were analyzed by northern blotting. *18S* rRNA ethidium bromide staining shows equal loading.

C. Relative reporter mRNA levels from panel B at time point zero (before ActD addition) were defined as 100%. Relative reporter mRNA levels were plotted as a function of time. Circles represent the mean value and error bars the standard deviation (SD) (n = 3). The decay curves were fitted to an exponential decay with a single component (dotted lines). R^2 values are indicated for each curve. The half-life of each mRNA in WT and DDX6 KO cells is represented as the mean ± SD.

D. HEK293T cells were transfected with MBP or POP2 dominant negative mutant (POP2 DE-AA) and indicated reporter plasmids. After 48 hr, cells were treated with ActD and harvested at the indicated time points. Reporter mRNA levels were analyzed by northern blotting. *18S* rRNA ethidium bromide staining shows equal loading.

E. Relative reporter mRNA levels from panel D at time point zero (before ActD addition) were defined as 100%. Relative reporter mRNA levels were plotted as a function of time. Circles represent the mean value and error bars the standard deviation (SD) (n = 3). The decay curves were fitted to an exponential decay with a single component (dotted lines). R^2 values are indicated for

each curve. The half-life of each reporter mRNA in WT and POP2 DE-AA overexpressing cells is represented as the mean ± SD.

Figure 2 DDX6 interacts with ribosomal proteins in human cells.

A. The interaction between the recombinant NusA-Strep-DDX6 and purified human ribosomal proteins was analyzed by SDS-PAGE and stained with Coomassie blue. Input lysate (1%) and bound fractions (20%) were loaded.

B. Western blot showing the interaction between GFP-tagged DDX6 full-length/N-ter/C-ter with HA-tagged RPL22 and endogenous RPS3A in human HEK293T cells. GFP-tagged MBP served as a negative control. For the GFP-tagged proteins, the HA-tagged RPL22 and the endogenous RPS3A, 1% of the input and 20% of the immunoprecipitate were loaded. N-ter: N-terminus; C-ter: C-terminus.

C. Immunoprecipitation assay showing the interaction of GFP-tagged DDX6 (wild-type or the indicated mutants) with HA-tagged RPL22 or endogenous CNOT1 in HEK293T cells. Samples were analyzed as described in B.

D. DDX6 KO HEK293T cells were transfected with the control R-LUC reporter or a reporter containing 30x rare codons and GFP-tagged DDX6 wild-type or mutants. After treating cells with ActD for 8 hr *R-LUC* mRNA levels were analyzed by northern blotting. *18S* rRNA ethidium bromide staining shows equal loading.

E. Relative control reporter mRNA levels from panel D were defined as 100%. Relative 30x rare codon reporter mRNA levels were plotted. Bars represent the mean value and error bars the standard deviation (n = 3).

F. Immunoblot illustrating the expression of proteins used in the assay shown in panel D.

Figure 3 DDX6 controls mRNA abundance and translational efficiency in human cells.

A. Comparative analysis of translational efficiency (TE) in wild-type (WT) HEK293T and DDX6 KO cells. Genes with significantly (FDR<0.005) increased (n=1707 genes) and decreased (n=1484 genes) mRNA abundance are colored in red and blue, respectively.

B. Comparative analysis of translational efficiency (TE) in WT HEK293T and DDX6 KO cells. Genes with significantly (FDR<0.005) increased (n=260 genes) and decreased (n=38 genes) TE are highlighted in salmon and cyan, respectively. The top 20 (total 89) of translationally upregulated zinc finger transcription factors in DDX6 KO cells are highlighted.

C. Pie charts indicating the fractions and absolute numbers of significantly (FDR<0.005) differentially expressed mRNAs in HEK293T WT and DDX6 KO cells as determined by RNA-seq.

D. Pie charts indicating the fractions and absolute numbers of significantly (FDR<0.005) differentially translated mRNAs in HEK293T WT and DDX6 KO cells as determined by Ribo-seq/RNA-seq.

E. Gene ontology of the biological processes associated with upregulated transcripts in DDX6 KO cells. Bar graph shows $\log_{10}$ q-values for each overrepresented category. Values and circles indicate the % of genes within each category.

F. Gene ontology of the biological processes associated with translationally upregulated transcripts in DDX6 KO cells. Bar graph shows $\log_{10}$ q-values for each overrepresented category. Values and circles indicate the % of genes within each category.

G. qPCR analysis of *AR* and *BMP2* mRNA levels in HEK293T WT and DDX6 KO and rescued with GFP-tagged DDX6 (wild-type or the indicated mutants). $\log_2$FC values for each transcript as determined by the RNA-seq experiments are indicated.

H. Immunoblot depicting the expression of proteins used in the assay shown in panel G.

Figure 4 DDX6 is required for ribosome-stalling mRNA degradation

A. Schematic representation of the reporters used in panels (B, C).

B. Representative northern blots showing the decay of *AR* reporter mRNAs in HEK293T wild-type (WT) or DDX6 KO cells. Cells were transfected with indicated reporter plasmids and monitored after the inhibition of transcription using actinomycin D (ActD) for the indicated time. *18S* rRNA ethidium bromide staining shows equal loading.

C. Relative reporter mRNA levels from panel B at time point zero (before ActD addition) were defined as 100%. Relative reporter mRNA levels were plotted as a function of time. Circles represent the mean value and error bars the standard deviation (SD) (n = 3). The decay curves were fitted to an exponential decay with a single component (dotted lines). R^2 values are indicated for

each curve. The half-life of each mRNA in WT and DDX6 KO cells is represented as the mean ± SD.

D. Representative northern blots showing the decay of *BMP2* reporter mRNAs in HEK293T WT or DDX6 KO cells. Cells were transfected with indicated reporter plasmids and monitored after the inhibition of transcription using actinomycin D (ActD) for the indicated time. *18S* rRNA ethidium bromide staining shows equal loading.

E. Relative reporter mRNA levels from panel D at time point zero (before ActD addition) were defined as 100%. Relative reporter mRNA levels were plotted as a function of time. Circles represent the mean value and error bars the standard deviation (SD) (n = 3). The decay curves were fitted to an exponential decay with a single component (dotted lines). R^2 values are indicated for each curve. The half-life of each mRNA in WT and DDX6 KO cells is represented as the mean ± SD.

F. HEK293T cells were transfected with indicated R-LUC reporters containing 6×MS2 binding sites, HA-tagged RPL22, and SBP-tagged MBP-MS2 plasmids. RNA bound to SBP-MBP-MS2 was immunoprecipitated with Streptavidin beads. The presence of HA-tagged RPL22 in the immunoprecipitates was determined by western blotting. SBP-MBP-MS2 protein level and RT-PCR of R-LUC reporter RNA levels served as a loading control.

SUPPLEMENTAL FIGURES

Figure S1 Characterization of HEK293T DDX6 KO cells

A. Immunoblots were probed with antibodies recognizing DDX6 and Tubulin.

B, C. Multidimensional scaling (MDS) analysis for the Ribo-Seq (B) and RNA-Seq (C) replicate libraries from HEK293T wild-type (WT) and DDX6 KO cells. The Ribo-Seq and RNA-Seq experiments were reproducible as replicates clustered together.

D. Sanger sequencing of the DDX6 genomic region targeted by the DDX6 sgRNA. Frameshift mutations were detected in exon 3 of both alleles. These generate premature STOP codons (PTC) and deletions in DDX6.

E. Ribosome footprints (RFP) and total mRNA (RNA) reads distribution along *DDX6* mRNA in wild-type (WT) and DDX6 KO cells. Of note, RFP and total RNA counts for DDX6 are drastically reduced in the KO cells.

Figure S2 Identification of DDX6 target mRNAs

A. Schematic representation of the experimental strategy to identify mRNAs targeted by DDX6 for translational repression and decay.

B-G. Ribosome footprints (RFP) and total mRNA (RNA) reads distribution along DDX6 target mRNAs in wild-type (WT) and DDX6 KO cells. Potential ribosome stalling sites are indicated in red dotted boxes.

Figure S3 Characterization of DDX6 target mRNAs

A. qPCR analysis of *LGALS1*, *DLX5*, *ENO2* and *PSMB9* mRNA levels in HEK293T wild-type (WT) and DDX6 KO and rescued with GFP-tagged DDX6 (wild-type or the indicated mutants). $\log_2$FC values for each transcript as determined by the RNA-seq experiments are indicated.

B-D. Ridgeline plots illustrating the GC content (B), coding sequence (CDS) length (C), and translational efficiency (TE) (E) of translationally regulated DDX6 target mRNAs. Statistical significance was calculated with the one-sided Wilcoxon rank sum test.

Weber *et al.* Figure 1

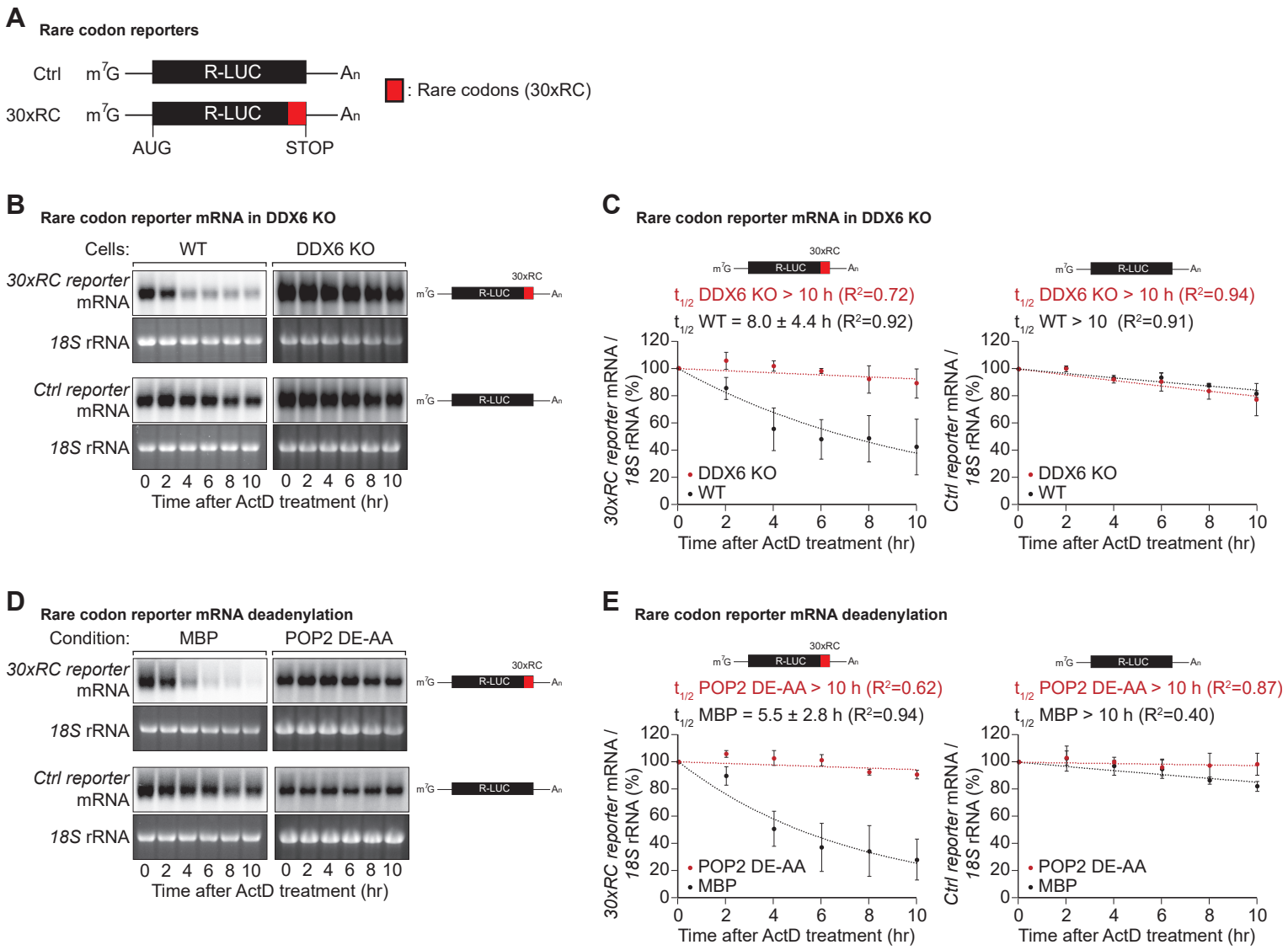

Weber *et al.* Figure 2

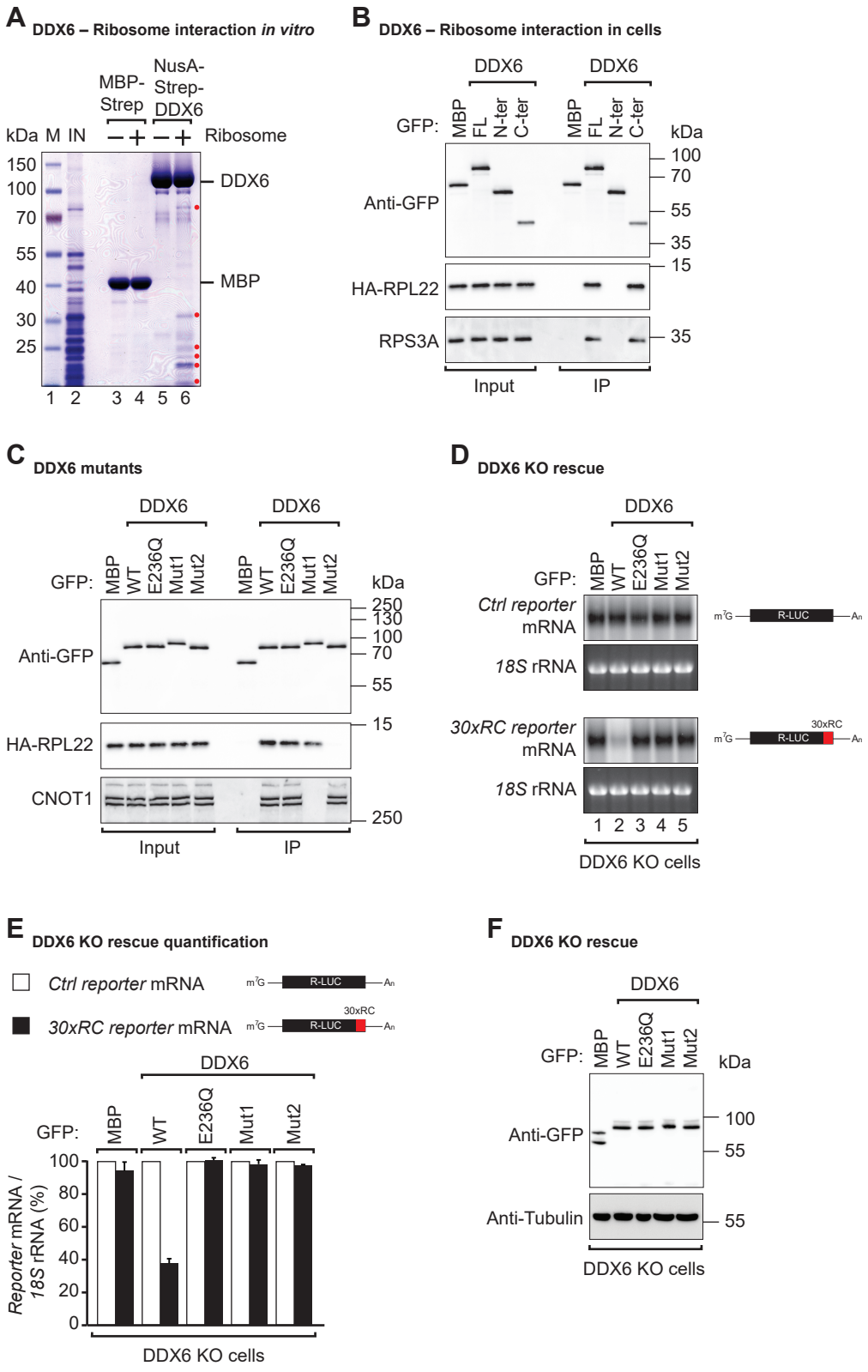

Weber *et al.* Figure 3

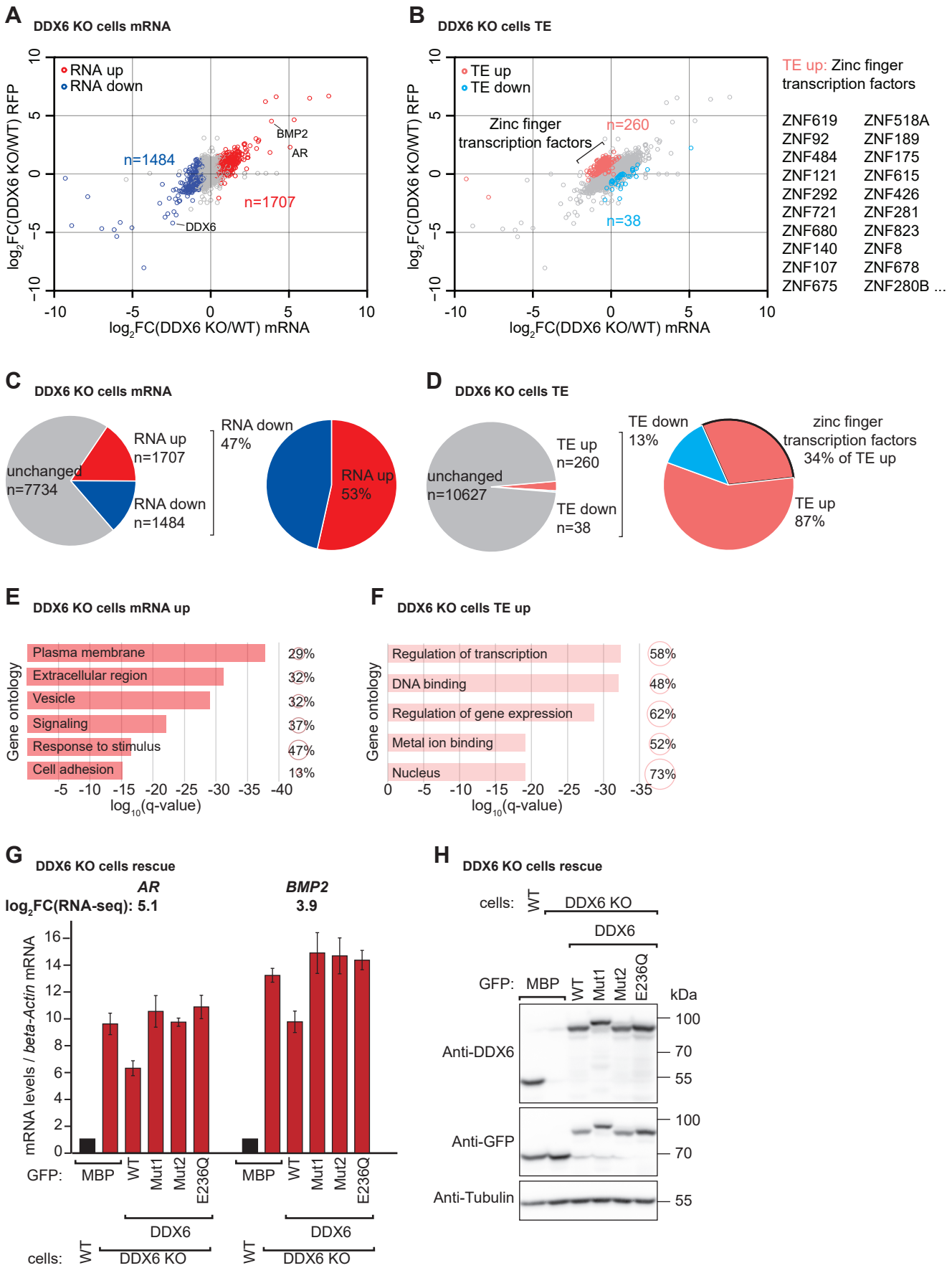
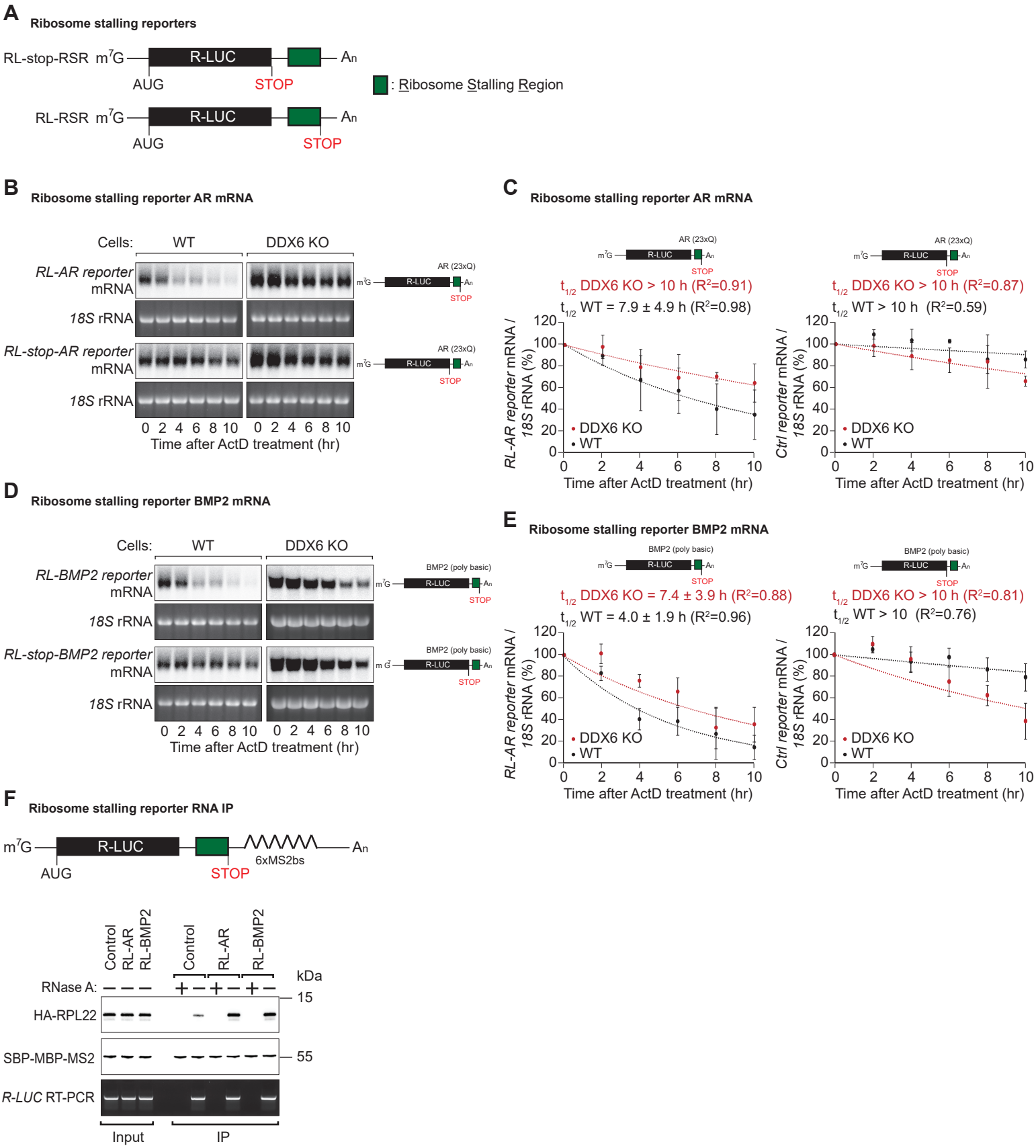
Weber *et al.* Figure 4